Journal of Hazardous Materials 384 (2020) 121382

Contents lists available at ScienceDirect

Journal of Hazardous Materials

journal homepage: www.elsevier.com/locate/jhazmat

Controllable incorporation of oxygen in MoS_2 for efficient adsorption of Hg^{2+} in aqueous solutions

Weiquan Zhan[a], Feifei Jia[b,*], Yuan Yuan[b], Chang Liu[b], Kaige Sun[a], Bingqiao Yang[c], Shaoxian Song[a,*]

[a] Hubei Key Laboratory of Mineral Resources Processing and Environment, Wuhan University of Technology, Luoshi Road 122, Wuhan, Hubei, 430070, China
[b] School of Resources and Environmental Engineering, Wuhan University of Technology, Luoshi Road 122, Wuhan, Hubei, 430070, China
[c] School of Xingfa Mining Engineering, Wuhan Institute of Technology, Xiongchu Avenue 693, Wuhan, Hubei, 430073, China

GRAPHICAL ABSTRACT

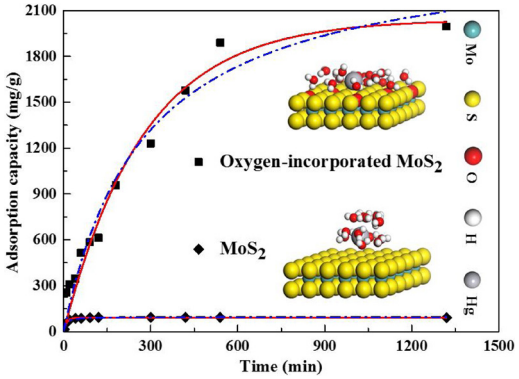

ARTICLE INFO

Editor: Daniel CW Tsang

Keywords:
Oxygen incorporation
MoS_2
Hg^{2+} adsorption
DFT calculations

ABSTRACT

Molybdenum disulfide (MoS_2) was incorporated controllably by oxygen in order to modify the hydrophobic surfaces and thus to improve the adsorption of Hg^{2+} on MoS_2 in aqueous solutions in this work. The experimental results indicated that the incorporation of oxygen could dramatically improve the adsorption of Hg^{2+} on MoS_2. With 11% oxygen atom incorporation, the adsorption rate and capacity increased over 17 times and 21 folds, respectively, compared with that without oxygen incorporation. This vast improvement was found to be contributed to that the incorporation of oxygen would greatly enhance the complexation between S atoms and Hg^{2+} on MoS_2 surfaces, resulting in the great increase of the Hg^{2+} adsorption. The increase of the adsorption capacity with increasing incorporated oxygen reached a plateau, which might be due to the saturation of covalent bond. In addition, the incorporation of oxygen atom greatly enhanced the hydrophilicity of MoS_2 surfaces, facilitating the hydrated Hg^{2+} ions to approach to MoS_2 surfaces. This finding might provide a highly potential adsorbent for efficiently removing Hg^{2+} from water.

* Corresponding authors.
E-mail addresses: feifeijia@whut.edu.cn (F. Jia), ssx851215@whut.edu.cn (S. Song).

https://doi.org/10.1016/j.jhazmat.2019.121382
Received 8 June 2019; Received in revised form 8 September 2019; Accepted 1 October 2019
Available online 03 October 2019
0304-3894/

1. Introduction

Mercury (Hg) pollution in aqueous solutions had been a worldwide environmental problem owing to its high toxicity (Obrist et al., 2017). As a great threat to public health, Hg caused serious human disease, known as minamata disease (Nanomi and David, 2013). Thus, it is critical to develop efficient technologies for removing Hg^{2+} from aqueous solution. Among the existing technologies of removing Hg^{2+}, adsorption is regarded as the most promising method in terms of its simplicity, regeneration capacity and cost efficiency (Kim et al., 2018; Vikrant and Kim, 2019).

During the past few years, various adsorbents had been exploited for removing Hg^{2+} from aqueous solution (Huang et al., 2019; Zhang et al., 2019; Di Natale et al., 2011). Conventional adsorbent materials like clays (Sdiri et al., 2012; Zhan et al., 2019), active carbon (Rao et al., 2009) had poor selectivity and weak binding affinity for Hg^{2+} removal. Recently, given strong soft-soft interactions between Hg^{2+} and sulfur, sulfur resources had been introduced into various materials, such as thiol-functionalized decorated metal organic frameworks (Shin et al., 2018; Xiao and Jiang, 2018), thiol-functionalized decorated covalent organic frameworks (He et al., 2018; Wibmer et al., 2018). But, these materials suffer from complex preparation step and expensive synthesized raw materials, which limited the practical application (Ai et al., 2016). Meanwhile, molybdenum disulfide (MoS_2) had received tremendous attentions because of its abundant intrinsic sulfur atoms, strong adsorption capacity and large specific surface area (Jia et al., 2017a, 2018; Liu et al., 2017a; Zhao et al., 2015; Peng et al., 2017; Yuan et al., 2019). As a typical layered transition-metal dichalcogenide, MoS_2 possessed layered structure with each layer consisting of one molybdenum sheet sandwiched by two sulfur sheets (Wang and Mi, 2017; Pető et al., 2018; Li and Peng, 2018). There is weak wan der Waals forces between individual sandwiched S-Mo-S layers, but strong chemical bonding within layers (Liu et al., 2014). Hence, MoS_2 is prone to form two-dimensional morphology that can offer large surface area for Hg^{2+} adsorption. According to the report (Liu et al., 2017b), the adsorption capacity of Hg^{2+} on natural molybdenite is 305 mg/g, which showed an improvement compared with other adsorbents. However, the surface of MoS_2 was hydrophobic, which was unfavorable for the hydrated Hg^{2+} bound with sulfur atoms exposed outside.

Based on the key factor, some attempts had been made focusing on the improvement of surface property of MoS_2 (Feng et al., 2017, 2019; Feng et al., 2018). In previous work (Jia et al., 2018), thermal treatment on MoS_2 was developed, leading to partial oxidation on the surface of MoS_2, which exhibited higher removal capacity of Hg^{2+}. Nevertheless, oxygen atoms were only on the outer most surface of MoS_2, limited Hg^{2+} adsorption on MoS_2. In addition, Mo^{VI} was introduced into MoS_2, which made the adsorbent instable and soluble in aqueous solution.

To overcome the instable structure of MoS_2 and improve the limited adsorption capacity of Hg^{2+} on MoS_2, elemental incorporation was put forward to realize the simultaneous optimization on improving the surface properties of MoS_2 and avoiding the introduction of Mo^{VI} for efficient Hg^{2+} removal. Oxygen atoms had a commendable affinity with water molecules and Hg^{2+}. Bearing the fact in mind, oxygen incorporation in MoS_2 might be an efficient method for removing Hg^{2+} from aqueous solution. In this work, an aim was made for researching the incorporation of oxygen in MoS_2 to explore the adsorption behavior and mechanism of oxygen-incorporated MoS_2 for removal Hg^{2+} from aqueous solution. X-ray diffraction (XRD), transmission electron microscopy (TEM) and X-ray photoelectron spectroscopy (XPS) were used for studying the properties of oxygen-incorporated MoS_2. The performances of Hg^{2+} adsorption on MoS_2 was investigated by kinetics experiments. The mechanism of the remarkable adsorption of Hg^{2+} on oxygen-incorporated MoS_2 was explained through XPS determination, as well as theoretical density functional theory (DFT) calculations. The objective was to understand more clearly about the influence of surface property of MoS_2 on removal of Hg^{2+} in aqueous solution, thus to pave a new way of MoS_2 as superb adsorbent for removing heavy ions.

2. Experimental

2.1. Materials

Mercuric nitrate ($Hg(NO_3)_2{\cdot}H_2O$) was purchased from Shanghai Zhanyun Chemical Co., Ltd (China), other chemicals were purchased from Sinopharm Chemical Reagent Co., Ltd. and used as received. Ultra-pure water (Millipore Super Q system) with a resistivity of 18.2 MΩ cm was used in the experiments.

2.2. Synthesis of oxygen-incorporated MoS_2

MoS_2 without oxygen incorporation could be synthesized at 220 °C for 24 h according to previous work (Xie et al., 2013a). Then oxygen-incorporated MoS_2 was prepared through controlling the process of crystallization by synthesis time. Typically, 2 mmol $(NH_4)_6Mo_7O_{24}{\cdot}4H_2O$ and 60 mmol thiourea were dissolved in 72 mL distilled water under vigorous stirring for 30 min. Then the solution was transferred into a 100 mL Teflon-lined stainless-steel autoclave and 220 °C for different time (i.e., 6–24 h). After the reaction system cooled down naturally to room temperature, the obtained products were collected by filtration, washed with water and ethanol, and dried under 60 °C in vacuum. In the work, all the products were named as SX, where X exhibits the synthesis time in hour.

2.3. Hg^{2+} adsorption experimental

Batch experiments were applied for studying the adsorption of Hg^{2+} on various oxygen-incorporated MoS_2. Adsorption kinetics of Hg^{2+} on various oxygen-incorporated MoS_2 were carried out in Hg^{2+} concentration of 125 mg/L and pH of 6.0 ± 0.1 (adjusted by NaOH or HNO_3). Firstly, 50 mg adsorbent was added into 1 L 125 mg/L Hg^{2+} solution. Then, the suspension was shaken and sealed in a water bath shaker at normal temperature and shaking rate of 150 rpm. After that, at different time intervals (0–1320 min), 5 ml suspension was filtered with 0.22 μm filter membrane, discarding the first 2 ml and leaving another 3 ml for analysis. The filtrates were then analyzed using a contrAA700 continuum source atomic adsorption spectrometry (AAS) system to detect the concentration of Hg^{2+}.

Hg^{2+} adsorption capacity was calculated by the following equation:

$$q = \frac{V_0 C_0 - CV}{m} \quad (1)$$

where q was the adsorption capacity of the adsorbent, mg/g; C_0 and C meant the Hg^{2+} concentration in the solution before and after adsorption, respectively, mg/L; V_0 and V represented the solution volume of the Hg^{2+} solution before and after adsorption, respectively, L; m was the mass of the adsorbent in the test, g.

2.4. Density functional theory (DFT) calculations

The detailed Hg^{2+} adsorption mechanism in oxygen-incorporated MoS_2 systems was handled at the level of DFT calculated by Dmol3 program (Material Studio 8.0 software). Oxygen atoms doping in MoS_2 monolayer was constructed by substituting sulfur atoms with similar number of oxygen atoms. Different concentrations of oxygen incorporation were investigated: zero, one, two, three and four of S atoms were substituted by O atoms and named MoS_2, MoS_2-O, MoS_2-2O, MoS_2-3O, MoS_2-4O, respectively. The models of Hg^{2+} adsorption on the surface of MoS_2 and oxygen-incorporated MoS_2 were built to investigate the isolated adsorption behavior of Hg^{2+} on the oxygen-incorporated MoS_2, which were shown in Figure S1. Hg^{2+} and H_2O molecules on the surface of MoS_2 and oxygen-incorporated MoS_2 were

built for researching the adsorption behavior of Hg^{2+} in the water system, as pictured in Figure S2. Periodic boundary conditions with a vacuum space of 20 Å was constructed to avoid the interaction between neighboring MoS_2 layers. The supercells consist of 2 × 2 × 1 unit cell for oxygen-incorporated MoS_2 systems was performed. The generalized gradient approximation (GGA), developed by Perdew-Bruker-Ernzerhof (PBE) was applied for accounting for exchange. A Monkhorst-Pack k-point mesh of 2 × 2 × 1 was used for sampling the Brillouin zone. The adsorption energies of Hg^{2+} and H_2O on the surface of adsorbents could be expressed by Eq. (2),(3), respectively. Similarly, Eq. (4) represented the interaction between H_2O molecules and Hg^{2+}.

$$\Delta E_{Adsorbent/Hg^{2+}} = E_{Adsorbent/Hg^{2+}} - E_{Adsorbent} \quad (2)$$

$$\Delta E_{Adsorbent/H_2O} = (E_{Adsorbent/n\cdot H_2O} - E_{n\cdot H_2O} - E_{Adsorbent})/n \quad (3)$$

$$\Delta E_{Hg^{2+}/H_2O} = (E_{Hg^{2+}/n\cdot H_2O} - E_{n\cdot H_2O})/n \quad (4)$$

where adsorbent represented MoS_2, MoS_2-O, MoS_2-2O, MoS_2-3O or MoS_2-4O; n was the number of H_2O molecules in the system; $\Delta E_{Adsorbent/Hg^{2+}}$ and $\Delta E_{Adsorbent/H_2O}$ were the adsorption energy between adsorbent and Hg^{2+} and H_2O, respectively; $\Delta E_{Hg^{2+}/H_2O}$ meant the interaction energy between Hg^{2+} and H_2O; $E_{Adsorbent/Hg^{2+}}$, $E_{Adsorbent/n\cdot H_2O}$, $E_{Adsorbent}$, $E_{Hg^{2+}/n\cdot H_2O}$ and $E_{n\cdot H_2O}$ were the energy of adsorbent-Hg^{2+} system, adsorbent-H_2O system, adsorbent system, Hg^{2+}-H_2O system and H_2O system, respectively.

2.5. Characterization

XRD was performed on a D8 Avance system with Cu K_α radiation (λ = 0.15406 nm). SEM images were taken on a Zeiss Ultra Plus for obtaining the morphology and the energy dispersive spectra (EDS). XPS was acquired on an ESCALB 250Xi photoelectron spectrometer. A contarAA700 continuum source atomic adsorption spectrometry system was used for detecting the concentration of Hg^{2+}. The high-resolution TEM (HRTEM) was performed on a Tecnai G^2 F30 S-TWIN transmission electron microscope.

3. Results and discussion

3.1. Characterization of oxygen-incorporated MoS_2

The structures of samples synthesized at different time were investigated through XRD, and the results are given in Fig. 1. The diffraction peaks of all the samples could be indexed to the crystalline planes of MoS_2 phase, indicating the successful synthesis of MoS_2. The corresponding d spacing of S12, S18 and S24 were around 6.2 Å, which was consistent with that of pristine 2H-MoS_2 (6.15 Å). While, the characteristic peaks of S6 had a slight left, reaching a corresponding d spacing of 6.8 Å. The results demonstrated that the crystallinity

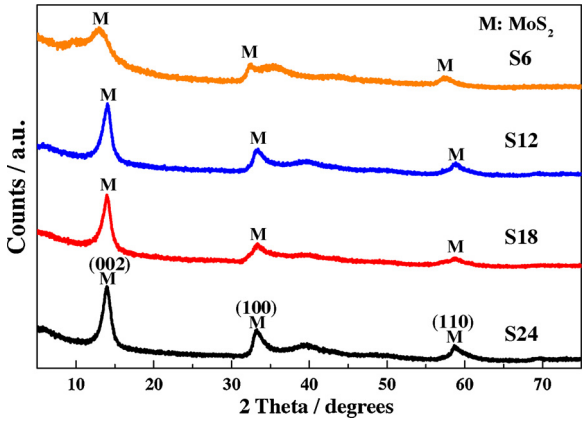

Fig. 1. XRD patterns of MoS_2 obtained at various time.

decreased with the decrease of synthesis time. And the inferior crystallinity of MoS_2 or the insufficient reduction of molybdate to molybdenum disulfide might result in the incorporation of oxygen atoms into the structure of MoS_2 (Xie et al., 2013a). All the prepared samples possessed almost same interlayer spacing, revealing that d spacing was not a dominant factor to affect the adsorption of Hg^{2+} on MoS_2.

SEM and TEM were used for characterizing the as-obtained oxygen-incorporated MoS_2. As Figure S3 outlined, all the samples exhibited ultrathin nanosheet morphology with uniform lateral size about 100–200 nm and showed obvious ripples, disclosing synthesis time did not affect the morphology and the ultrathin nature of the nanosheets (Xie et al., 2013b). When synthesis time decreased, the edges of nanosheets became obscurer, suggesting the lower crystallinity of the products. Cross-sectional TEM images (Figure S3d_1-d_4) of the curled edges of all the long time synthesized nanosheets (S12, S18, S24) exhibited the interlayer spacing were almost about 6.20 Å, low time synthesized nanosheets (S6) suggested expanded interlayer spacing of 6.76 Å, all results were consistent with the results from XRD analysis.

XPS and elemental mapping analyses were carried out for investigating the chemical composition of the products. XPS survey spectra of oxygen incorporated MoS_2 synthesized at various time was displayed at Figure S4, revealing the existence of Mo, S and O in S6, S12 and S18, but only Mo and S peaks observed in S24. Binding energy of Mo and O was consistent with that MoS_2, indicating the successful preparation of MoS_2. As shown in Fig. 2a_1-a_4, two characteristic peaks of Mo appeared at around 229 and 232 eV, arising from Mo $3d_{5/2}$ and Mo $3d_{3/2}$ orbitals, demonstrating the dominant existence of $Mo^{(IV)}$ in all the samples (Zhang et al., 2017). No peaks were found at around 235 eV, showing no Mo^{VI} was introduced in MoS_2, which indicated the prepared samples were in good stable structure. And S 2p region (Fig. 2b_1-b_4) represented two peaks with the $2p_{1/2}$ and $2p_{3/2}$ peak at about 162 and 163 eV, respectively, which was consistent with the S^{2-} of MoS_2 (Sun et al., 2017). In addition, the peak located at around 530 eV in the O 1s core-level spectrum (Fig. 2c_2-c_4) could be assigned to the incorporation of oxygen into MoS_2, which was attributed to the oxygen in the $Mo^{(IV)}O_2$ (Liu et al., 2016; Huang et al., 2015). The peak observed at 532 eV (Fig. 2c_2) could be assigned the adsorbed water (Moo et al., 2011; Jia et al., 2017b). No peaks of O 1s are observed in Fig. 2c_1, indicating that MoS_2 without oxygen incorporation could be obtained at the synthesis time of 24 h. Furthermore, the SEM image and corresponding EDS mapping analyses (Figure S5a-d) of an individual oxygen-incorporated MoS_2 showed the homogeneous distribution of the element of Mo, S and O in the whole oxygen-incorporated MoS_2. Detailed oxygen concentration in compositional analysis detected by both XPS and EDS is shown in Fig. 3, revealing that the atom concentration varied from 0% to 11% as the synthesis time decreased. It seemed that MoS_2 with more oxygen incorporation could be synthesized through controlling synthesis time, compared with control of synthesis temperature (Xie et al., 2013a). All of the results indicated the successful preparation of oxygen-incorporated MoS_2 and different concentration of oxygen atoms of oxygen-incorporated MoS_2.

3.2. Adsorption of Hg^{2+} on oxygen-incorporated MoS_2

Adsorption kinetics of Hg^{2+} on various oxygen-doping MoS_2 is shown in Fig. 4a. It could be seen that the adsorption increased quickly at initial time until it reached a plateau for all the MoS_2 adsorbents. It was obvious that S24 exhibited the lowest adsorption capacity at 93.11 mg/L. With increased O atoms brought in MoS_2, it showed continually enhanced Hg^{2+} adsorption capacity. After O atoms concentration reached to 11%, S6 showed the largest adsorption capacity at 1995.72 mg/L, which was almost 21 times than S24. The above results indicated that O atoms doping MoS_2 significantly improved the Hg^{2+} adsorption capacity. A pseudo-first-order kinetic model and a pseudo-second-order kinetic model were used to simulate the experimental data for investigating the mechanism of adsorption. The fitting

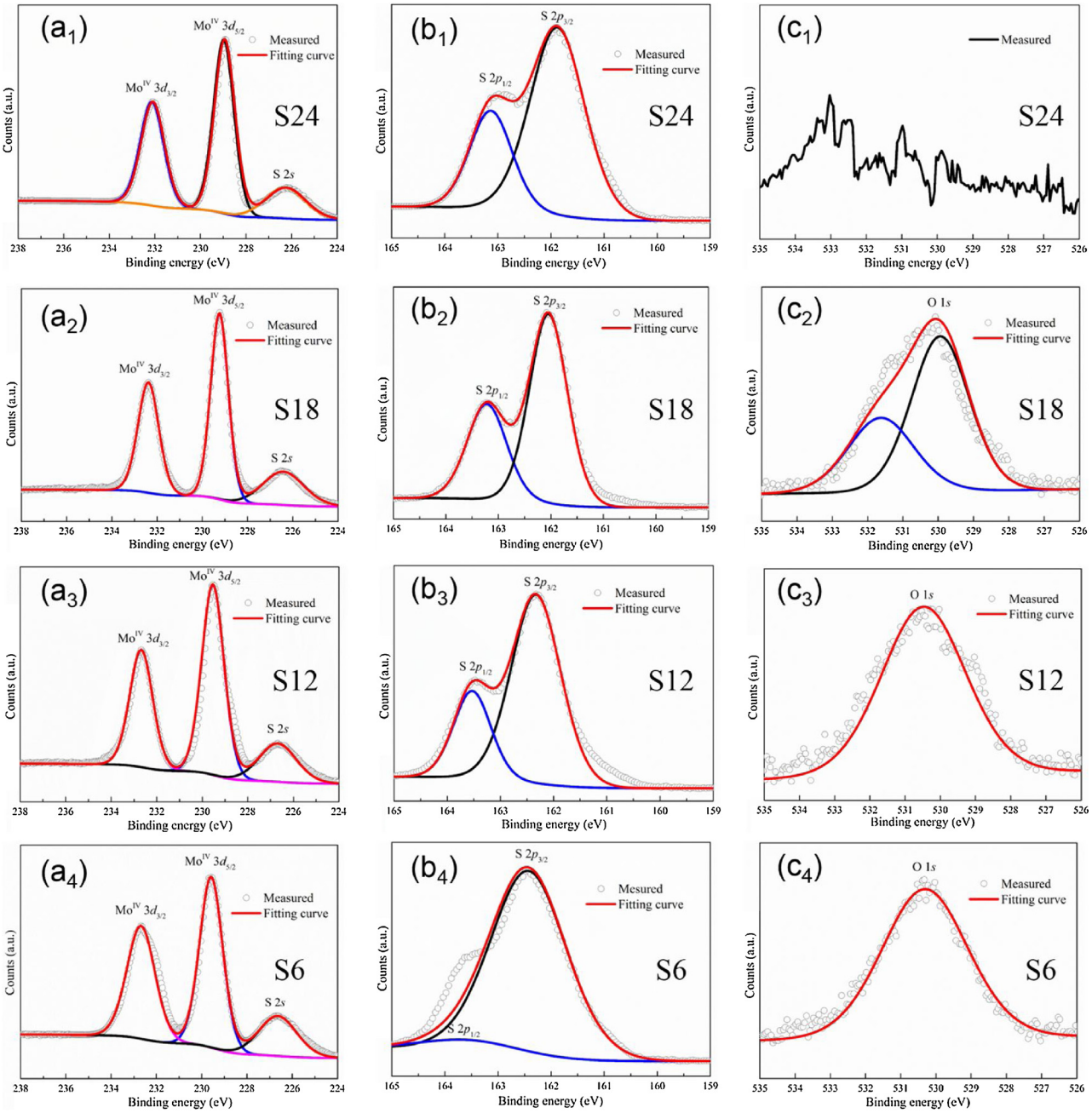

Fig. 2. XPS spectra exhibiting the binding energies of Mo (a_1-a_4), S (b_1-b_4), O (c_1-c_4) of the oxygen-incorporated MoS_2 synthesized at various times.

consequences were given in Table S1. Hg^{2+} adsorption on all the samples was well described by the pseudo-second-order kinetic model owing to the higher correlation coefficient of R_2^2, which might exist chemical sorption or chemisorption involving valence forces through sharing or exchanging of electrons between adsorbent and adsorbate. In other words, it demonstrated that chemical interaction might exist between Hg^{2+} and oxygen-incorporated MoS_2.

The initial adsorption rate (defined as the adsorbed Hg^{2+} per gram of the adsorbent per unit time on the adsorbent in the first 2 min) was used for evaluating the influence of O atoms doping MoS_2 on the adsorption kinetics of Hg^{2+}, which was illustrated in Fig. 4b. With increased concentration of O atoms in MoS_2, the initial adsorption rate increased. The adsorption rate of S6 was 122.5 mg g^{-1} min^{-1}, which was 17.3 times faster than that S24, further proving the dramatic effect of O atoms on the Hg^{2+} removal with MoS_2 as adsorbent.

SEM-EDS was performed on further confirming Hg^{2+} adsorption on oxygen-incorporated MoS_2. Figure S6 showed the EDS elemental mapping of Mo, S, O, Hg on the surface of oxygen-incorporated MoS_2 after Hg^{2+} adsorption at an initial concentration of 125 mg/L for 24 h. Elemental mercury was distributed evenly on the surface of adsorbent, indicating good adsorption of Hg^{2+} on the surface of oxygen-incorporated MoS_2. Fig. 5 displays the detailed Hg concentration in compositional analysis detected by both XPS and EDS. With increased concentration of O atoms in MoS_2, Hg concentration on MoS_2 increased, which means Hg^{2+} adsorption capacity on MoS_2 was improved. Meanwhile, the difference between the O concentration and Hg concentration might originate from the enhanced complexation between S atoms and Hg^{2+} on MoS_2 surfaces owing to oxygen atoms.

XPS was conducted to understand the immobilization mechanism of Hg^{2+} on oxygen-incorporated MoS_2 synthesized at various time. Elemental peaks of Mo, S, O and Hg were detected in Figure S7, strong peaks of Hg demonstrated adsorption of mercury on oxygen-

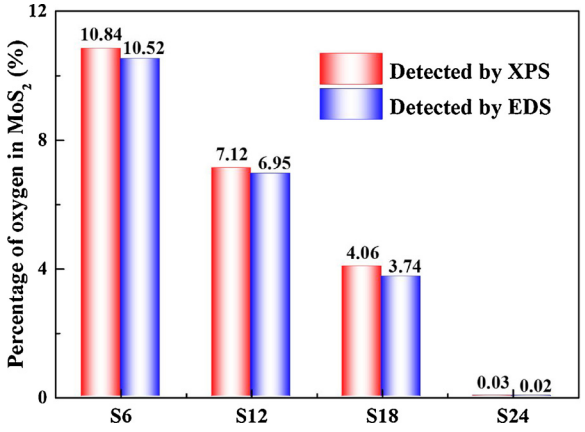

Fig. 3. Elemental analyses of the oxygen concentration in the oxygen-incorporated MoS_2.

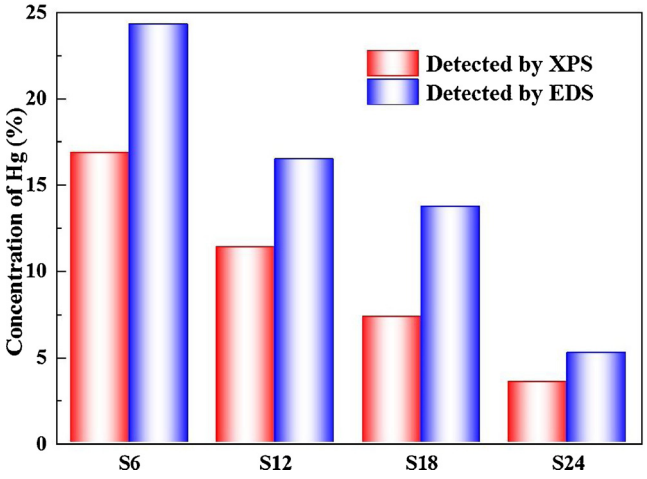

Fig. 5. Elemental analyses of Hg concentration after Hg^{2+} adsorbed on oxygen-incorporated MoS_2.

incorporated MoS_2. Fig. 6a_1-c_1 shows Hg 4f spectrum of Hg^{2+} adsorption on oxygen-incorporated MoS_2, spectra of Hg $4f_5$ and Hg $4f_7$ were separated into two peaks Strong peaks. The peak of Hg^0 at around 99.9 eV(Jia et al., 2017b) did not appear, demonstrating that no reduction of Hg^{2+} during the adsorption process. The doublet peak at around 100.7 and 104.8 eV were believed to HgS (Hyland et al., 1990), while another doublet at around 102.0 and 106.0 eV are assigned to HgO (Yeong et al., 2010), which demonstrated strong interaction between Hg^{2+} and oxygen-incorporated MoS_2. But, there was no peak of HgO appeared in the Hg^{2+} adsorption on MoS_2, which showed in Fig. 6d_1. The formation of HgS and HgO could be inferred from the great affinity between Hg^{2+} and adsorbent. In addition, the spectrum of S 2p is given in Fig. 6a_2-d_2, which might be assigned into MoS_2 peak at 161.9 and 163.5 eV, HgS peak at 161.7 eV (Zeng et al., 2001). Also, the spectrum of O1 s of S6, S12 and S18 are shows in Fig. 6b_3-c_3, which could be divided into two peaks, while no peak occurred in the spectrum of O1 s of S24 (Figure a_3). Peak at 530.3 eV was assigned to O 1s of MoO_2, while peak at 532.6 eV corresponded to O 1s of HgO (Jia et al., 2018). Therefore, the oxygen atoms on the surface of MoS_2 could greatly interact with Hg^{2+}.

3.3. DFT calculation for mechanism of Hg^{2+} adsorption

3.3.1. Interact energy between H_2O, Hg^{2+} and oxygen-incorporated MoS_2

DFT calculation was performed on exploring the detailed mechanism of Hg^{2+} adsorption on oxygen-incorporated MoS_2. The adsorption energies of both isolated Hg^{2+} and Hg^{2+} in water system on the surface of adsorbent was studied through exploring the interface interaction, as shown in Fig. 7a. With the introduction of oxygen atoms on MoS_2, the calculated adsorption energy of Hg^{2+} on the surface of MoS_2 increased sharply no matter in isolated adsorption or water system. Higher adsorption energy of Hg^{2+} on oxygen-incorporated MoS_2 in water system than that in isolated adsorption Hg^{2+} system, but opposite in Hg^{2+} adsorption on the surface of MoS_2. It could be ascribed that oxygen atoms on the surface of MoS_2 exhibited more powerful affinity to Hg^{2+} than sulfur atoms on the surface of MoS_2 due to the stronger electronegativity of oxygen atoms. What was more interesting, the adsorption energy of Hg^{2+} on oxygen-incorporated MoS_2 increased to balanced value with increasing oxygen incorporation concentrations. The phenomenon might be occurred originated from the saturation interaction between Hg^{2+} and oxygen-incorporated MoS_2. Also, water molecules had impact on the Hg^{2+} adsorption on the surface of adsorbent, promoting Hg^{2+} adsorption on oxygen-incorporated MoS_2 but weakening Hg^{2+} adsorption on MoS_2. For illustrating the phenomenon, interact energy between Hg^{2+} and H_2O, adsorbent and H_2O were calculated (Fig. 7b). As seen, the adsorption of H_2O on MoS_2 was 0.245 eV (an endothermic reaction), demonstrating repulsion between H_2O and MoS_2 (Zhao et al., 2014). Hg^{2+} showed good adsorption energy with H_2O molecules because of the hydration of Hg^{2+}. When oxygen atoms were introduced into MoS_2, the affinity of H_2O with MoS_2 was greatly improved. As a result, as oxygen incorporation, the adsorbed water molecule could accelerate Hg^{2+} approach to the surface of MoS_2, thus Hg^{2+} well interacted with sulfur and oxygen atoms.

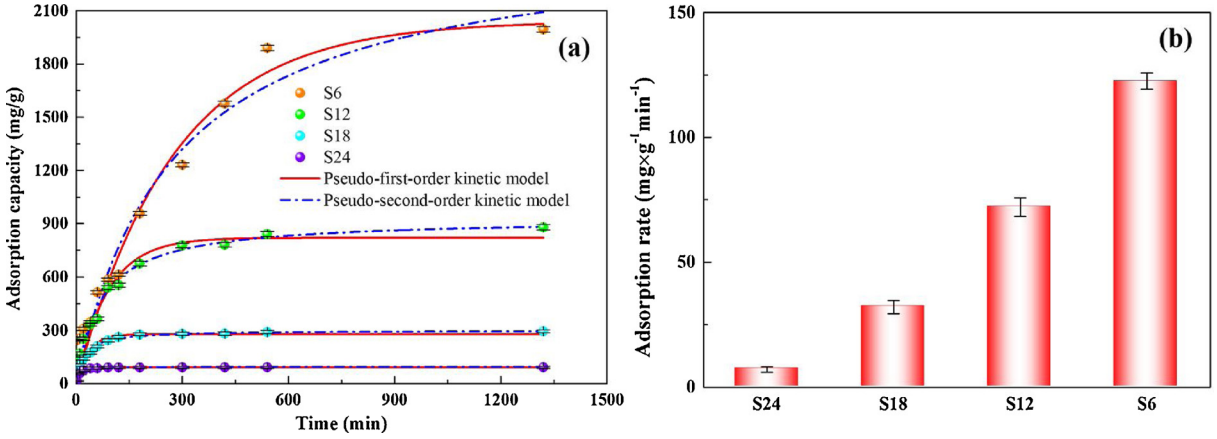

Fig. 4. Adsorption kinetics of Hg^{2+} on MoS_2 and oxygen-incorporated MoS_2, (a) adsorption capacity as a function of time, (b) adsorption rate in the first 2 min.

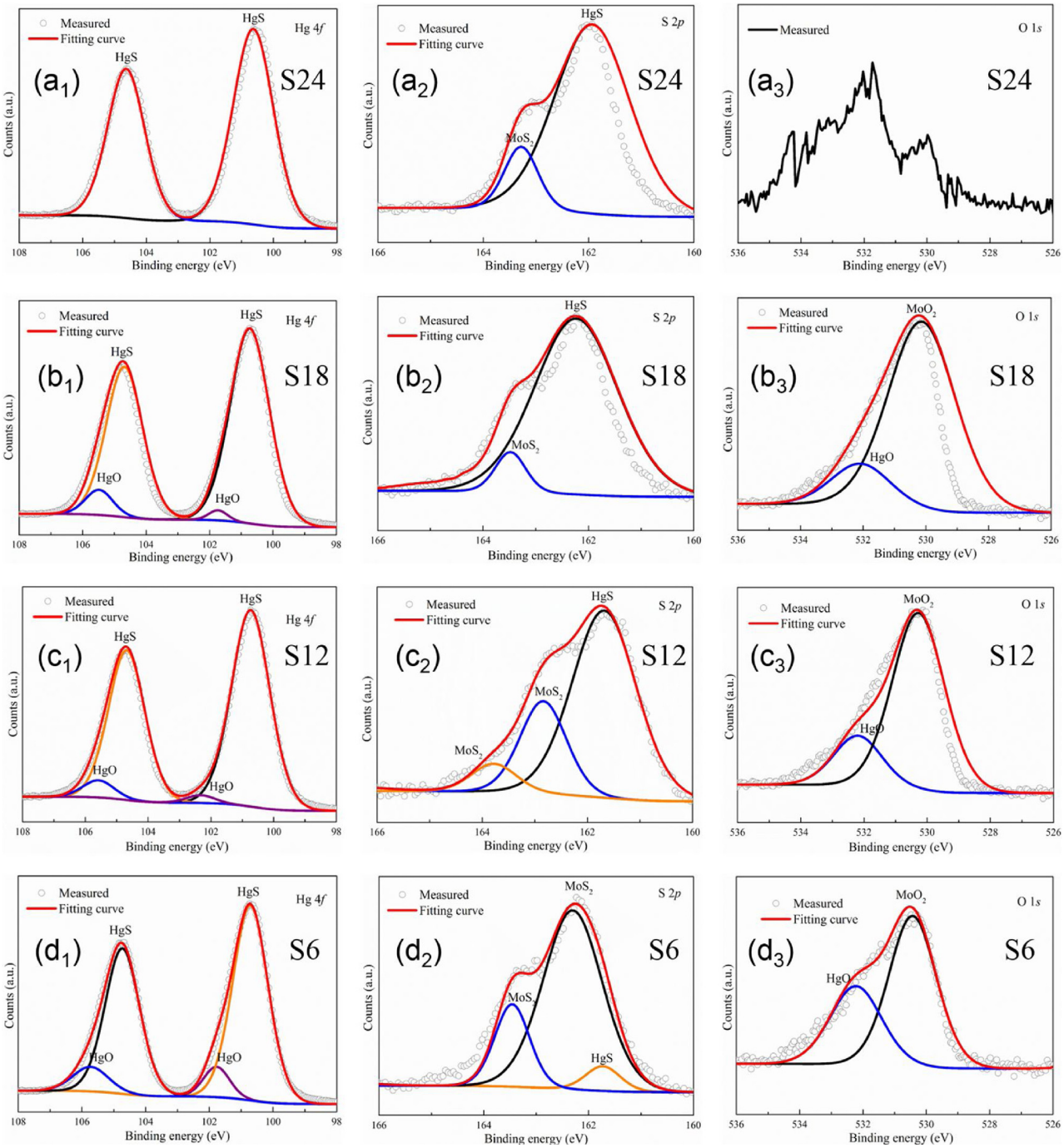

Fig. 6. XPS spectra of Hg^{2+} adsorption on the oxygen-incorporated MoS_2 synthesized at various time, (a_1-d_1) Hg 4f spectrum, (a_2-d_2) S 2p spectrum, (a_3-d_3) O 1s spectrum.

3.3.2. Electron density maps

Furthermore, the electron density maps of Hg^{2+} in water system adsorption on MoS_2 and oxygen-incorporated MoS_2 are shown in Fig. 8. In system of Hg^{2+} adsorption on MoS_2 (Fig. 8a), there existed very sparser overlap of electron cloud between Hg^{2+} and MoS_2, however dense overlap existed between Hg^{2+} and H_2O, which indicated the strong affinity of Hg^{2+} to H_2O but not to MoS_2. As for Hg^{2+} adsorption on oxygen-incorporated MoS_2 (Fig. 8b), overlap existed between Hg^{2+} and oxygen atoms from both H_2O and oxygen-incorporated MoS_2. Compared with H_2O, Hg^{2+} had more competitive ability to bind with the oxygen atoms on the surface of oxygen-incorporated MoS_2. Interestingly, dense overlap could be found between Hg^{2+} and sulfur atoms after the introduction of oxygen atom on MoS_2. It could be explained that when H_2O was attracted to the surface of oxygen-incorporated MoS_2, H_2O would drag Hg^{2+} close too. Then the closer Hg^{2+} interacted with sulfur and oxygen atoms on the surface of MoS_2. The results were consistent with those obtained from adsorption energies.

3.3.3. Partial density of states and Milliken atomic charge changes

In addition, the partial density of states (PDOS) was calculated for clarifying the interaction mechanism of between Hg^{2+}, H_2O, and MoS_2. For the Hg^{2+} adsorption on the surface of oxygen-incorporated MoS_2 in water system, the PDOS of the interaction between Hg^{2+} and O_W (oxygen atoms of H_2O molecules), H_W (hydrogen atoms of H_2O molecules) and O_M (oxygen atoms on the surface of MoS_2), Hg^{2+} and O_M, as well as Hg^{2+} and S_M (sulfur atoms on the surface of MoS_2) are plotted

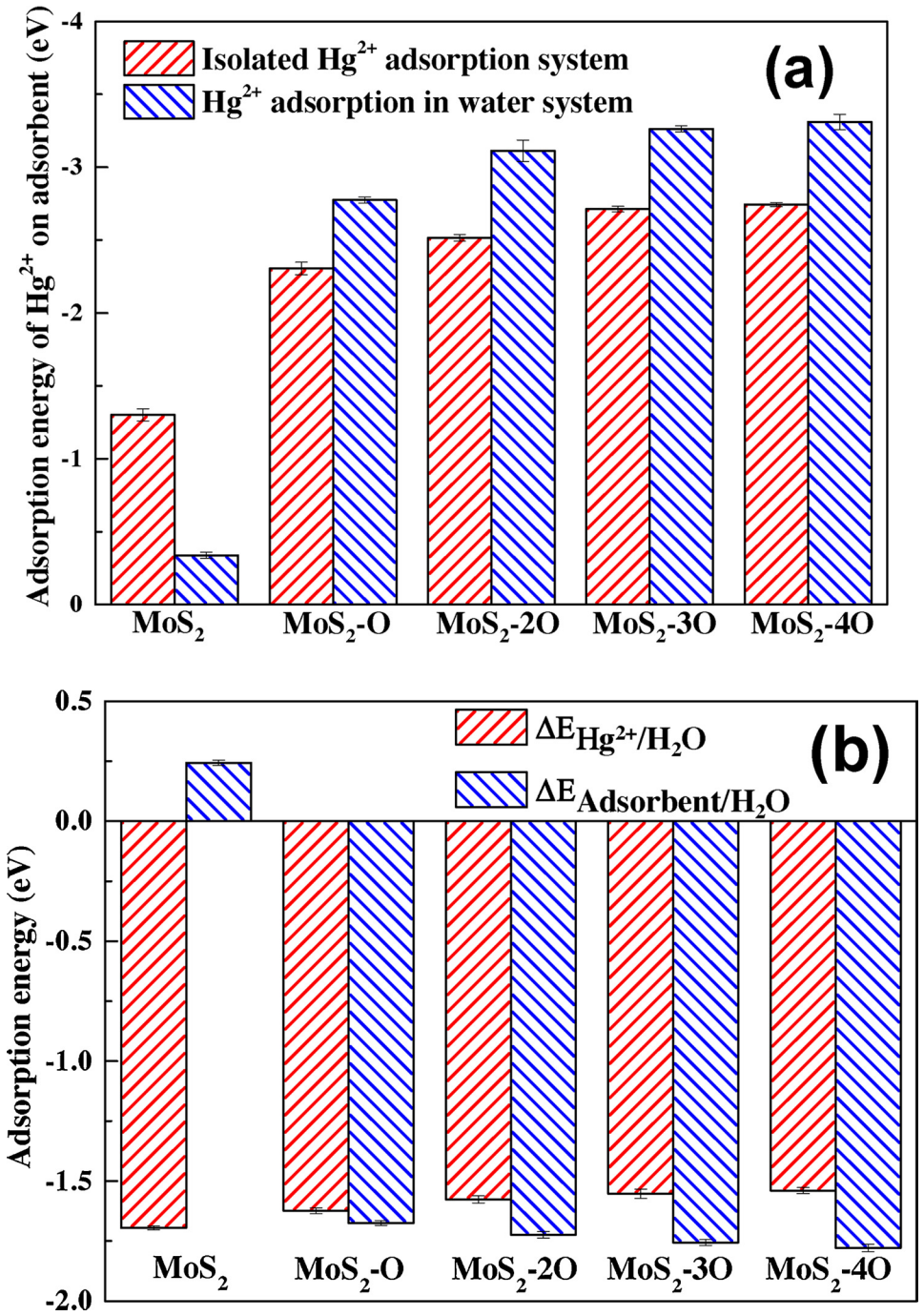

Fig. 7. Adsorption energy, (a) interact energy of adsorbent and Hg^{2+} in the system of isolated and water system, (b) interact energy of Hg^{2+} and H_2O and interact energy of adsorbent and H_2O in the water system.

in Fig. 9. As shown, the orbitals of Hg distributed mainly in the valence band not in the conduction band, showing that Hg atom strongly participated bonding interaction. As shown, the orbitals of Hg distributed mainly in the valence band instead of in the conduction band, showing that Hg atom strongly participated bonding interaction. It could be found that there was bonding between Hg 5d orbitals and O_W 2p orbitals in the range of −10 to −5 eV (Fig. 9a), but bonding was not stronger than that between Hg 5d orbitals and O_M 2p orbitals (Fig. 9b), which meant the strong interaction between Hg and oxygen atoms on the oxygen-incorporated MoS_2. Bonding between Hg 5d orbitals and S_W 3p orbitals was also found (Fig. 9c), exhibiting the interaction between Hg and sulfur atom on the surface of oxygen-incorporated MoS_2. As showed in Fig. 9d, there existed much overlap between H_W 1 s and O_M orbitals, suggesting the interaction between H_W and O_M should be hydrogen bonding.

Milliken atomic charge changes (ΔQ) of Hg^{2+}, O_W, O_M and S_M were calculated before and after the adsorption of Hg^{2+} to investigate the charge donors for Hg^{2+} in water system in Fig. 10. Positive value of charge changes (ΔQ) indicated the loss of electrons while negative value meant the obtain of electrons (Peng et al., 2016). It was found that Hg^{2+} was positively charged after adsorption, and the major lost charges transferred to the most nearby O_M, S_M and O_W. O_M obtained most electrons from Hg^{2+}, which meant that the electron of Hg^{2+} was transferred to oxygen atoms on the surface of MoS_2. Similarly, negative charge of O_M was more than that of S_M, indicating the interaction between O_M and Hg^{2+} was stronger than that between S_M and Hg^{2+}.

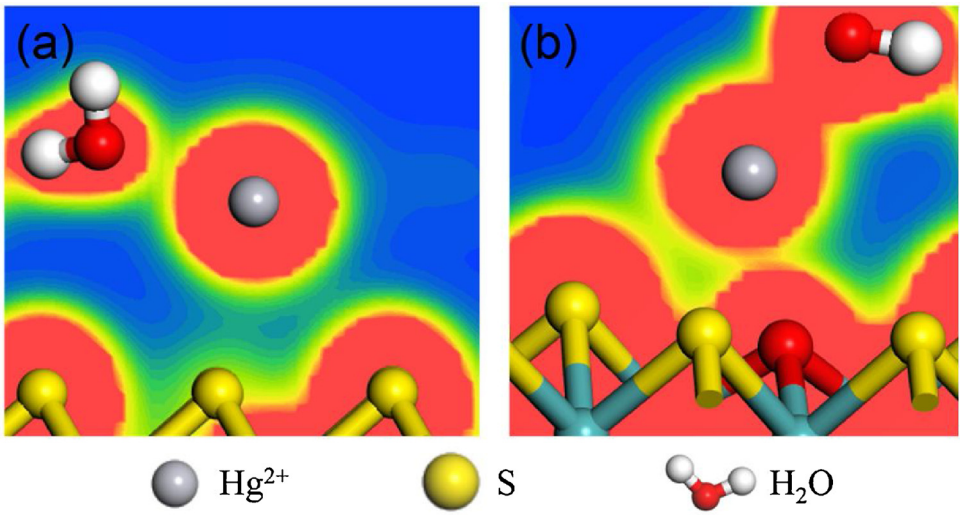

Fig. 8. Electron density maps of Hg^{2+} in water system on MoS_2 (a) and an individual oxygen-incorporated MoS_2 (b).

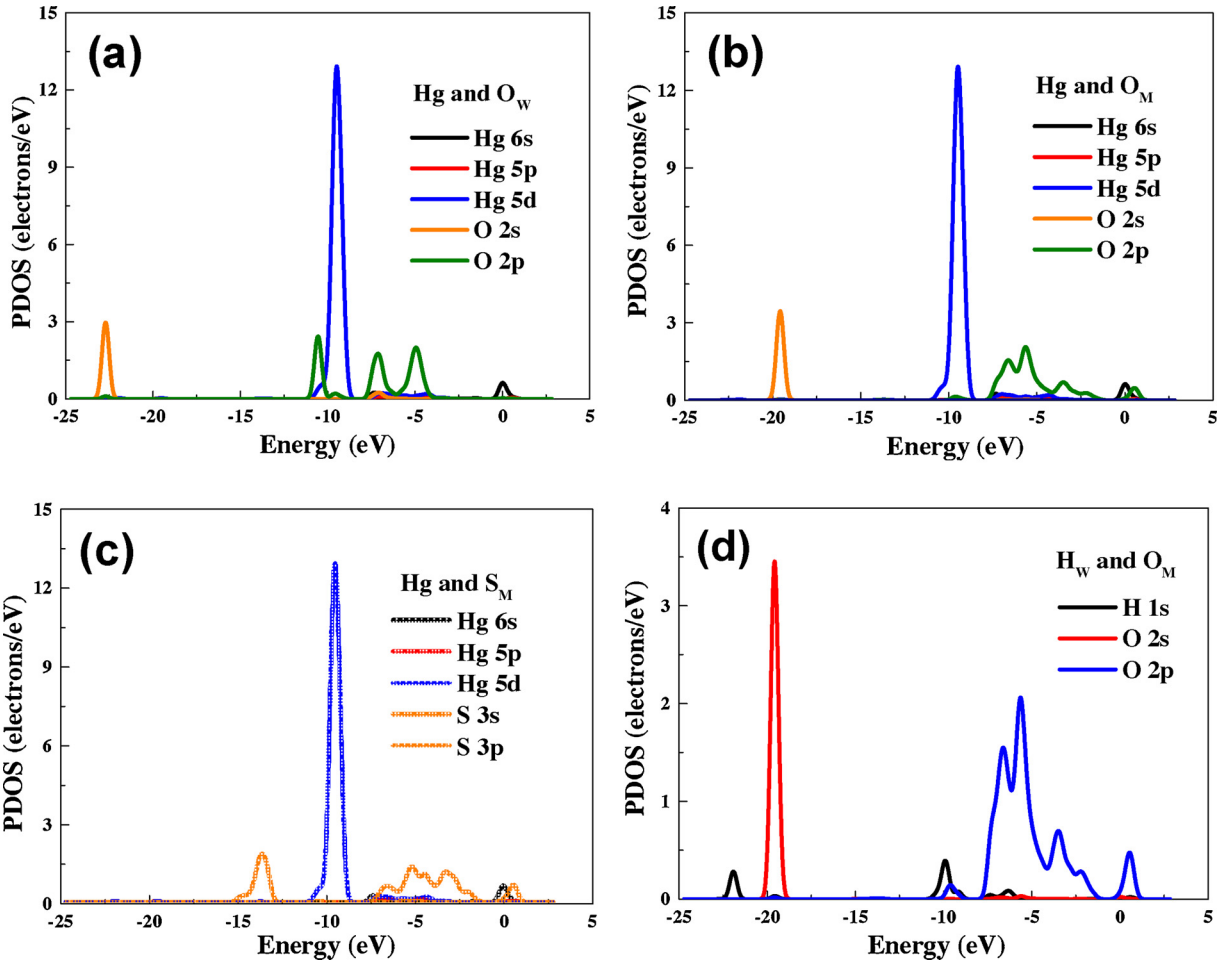

Fig. 9. PDOS for the Hg^{2+} adsorption on the surface of oxygen-incorporated MoS_2 in water system, (a) between Hg^{2+} and O_W; (b) between Hg^{2+} and O_M; (c) Hg^{2+} and S_M; (d) between H_W and O_M.

More interestingly, as the concentration of oxygen incorporation increased, charges transferred quickly, and then flatted might result from the saturation of covalent bond property. Meanwhile, S_M interacted strong with Hg^{2+} with the introduction of oxygen in MoS_2. The results demonstrated oxygen incorporated MoS_2 could enhance the interaction between Hg^{2+} and sulfur atom, and the capability of Hg^{2+} adsorption on oxygen-incorporated MoS_2 would reach equilibrium because of the saturation of covalent bond property.

4. Conclusions

In summary, oxygen incorporation in MoS_2 was firstly achieved by

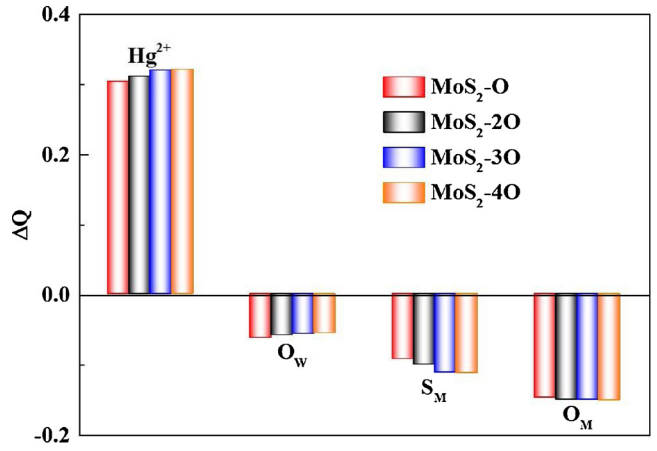

Fig. 10. Milliken atomic charges changes of Hg^{2+}, O_W, O_M and S_M in systems of Hg^{2+} adsorption on different Oxygen-incorporated MoS_2.

controlling the synthesized time, as decrease of the synthesized time, the concentration of oxygen increased. Oxygen-incorporated MoS_2 exhibited dramatical adsorption capacity of Hg^{2+} on MoS_2. After oxygen concentration reached to 11%, oxygen-incorporated MoS_2 showed 17.3 times faster and 21 folds higher on the adsorption capacity compared with MoS_2. As the introduction in MoS_2, affinity between Hg^{2+} and MoS_2 was greatly improved. Thus hydrated Hg^{2+} got closer to the surface of MoS_2, then bound with sulfur and oxygen atoms in MoS_2. Binding energy between Hg^{2+} and sulfur atoms in MoS_2 could be enhanced when oxygen was incorporated in MoS_2. The concentration of oxygen in MoS_2 increased, ability of Hg^{2+} adsorption on MoS_2 would reach stabilization because of covalent bond property. This work will broaden our vision to improve the removal of heavy ions in aqueous solution by structural modulations.

Acknowledgements

The financial supports to this work from the National Natural Science Foundation of China (No. 51704212, 51704220 and 51674183), the Natural Science Foundation of Hubei Province (No. 2016CFA013), and the Research Fund Program of Key Laboratory of Rare Mineral, Ministry of Land and Resources (KLRM-KF201802) are gratefully acknowledged.

Appendix A. Supplementary data

Supplementary material related to this article can be found, in the online version, at doi:https://doi.org/10.1016/j.jhazmat.2019.121382.

References

Obrist, D., Agnan, Y., Jiskra, M., Olson, C.L., Dominique, P., 2017. Tundra uptake pf atmospheric elemental mercury drives Arctic mercury pollution. Nature 547, 201–204. https://doi.org/10.1038/nature22997.

Nanomi, L., David, M., pliiution, Mercury, 2013. With pact's completion, the real work begins. Science (80-.) 341, 1443–1445.

Kim, Y., Lin, Z., Jeon, I., Van Voorhis, T., Swager, T.M., 2018. Polyaniline nanofiber electrodes for reversible capture and release of mercury(II) from water. J. Am. Chem. Soc. 140, 14413–14420. https://doi.org/10.1021/jacs.8b09119.

Vikrant, K., Kim, K.H., 2019. Nanomaterials for the adsorptive treatment of Hg(II) ions from water. Chem. Eng. J. 358, 264–282. https://doi.org/10.1016/j.cej.2018.10.022.

Huang, Y., Xia, S., Lyu, J., Tang, J., 2019. Highly efficient removal of aqueous Hg2+ and CH3Hg+ by selective modification of biochar with 3-mercaptopropyltrimethoxysilane. Chem. Eng. J. 360, 1646–1655. https://doi.org/10.1016/j.cej.2018.10.231.

Zhang, D., Wang, L., Zeng, H., Yan, P., Nie, J., Sharma, V.K., Wang, C., 2019. A three-dimensional macroporous network structured chitosan/cellulose biocomposite sponge for rapid and selective removal of mercury(II) ions from aqueous solution. Chem. Eng. J. 192–202. https://doi.org/10.1016/j.cej.2019.01.127.

Di Natale, F., Erto, A., Lancia, A., Musmarra, D., 2011. Mercury adsorption on granular activated carbon in aqueous solutions containing nitrates and chlorides. J. Hazard. Mater. 192, 1842–1850. https://doi.org/10.1016/j.jhazmat.2011.07.021.

Sdiri, A., Higashi, T., Chaabouni, R., Jamoussi, F., 2012. Competitive removal of heavy metals from aqueous solutions by montmorillonitic and calcareous clays. Water Air Soil Pollut. 223, 1191–1204. https://doi.org/10.1007/s11270-011-0937-z.

Zhan, W., Zhao, Y., Yuan, Y., Yi, H., Song, S., 2019. Development of 2D-Mt/SA/AgNPs microencapsulation phase change materials for solar energy storage with enhancement of thermal conductivity and latent heat capacity. Sol. Energy Mater. Sol. Cells 201, 110090. https://doi.org/10.1016/j.solmat.2019.110090.

Rao, M.M., Reddy, D.H.K.K., Venkateswarlu, P., Seshaiah, K., 2009. Removal of mercury from aqueous solutions using activated carbon prepared from agricultural by-product/waste. J. Environ. Manage. 90, 634–643. https://doi.org/10.1016/j.jenvman.2007.12.019.

Shin, H., Kim, J., Kim, D., Nguyen, V.H., Lee, S., Han, S., Lim, J., Char, K., 2018. Aqueous "polysulfide-ene" polymerization for sulfur-rich nanoparticles and their use in heavy metal ion remediation. J. Mater. Chem. A Mater. Energy Sustain. 6, 23542–23549. https://doi.org/10.1039/c8ta05457f.

Xiao, J.D., Jiang, H.L., 2018. Metal-organic frameworks for photocatalysis and photothermal catalysis. Acc. Chem. Res. 52, 356–366. https://doi.org/10.1021/acs.accounts.8b00521.

He, Y., Hou, Y.L., Wong, Y.L., Xiao, R., Li, M.Q., Hao, Z., Huang, J., Wang, L., Zeller, M., He, J., Xu, Z., 2018. Improving stability against desolvation and mercury removal performance of Zr(IV)-carboxylate frameworks by using bulky sulfur functions. J. Mater. Chem. A Mater. Energy Sustain. 6, 1648–1654. https://doi.org/10.1039/c7ta06118h.

Wibmer, L., Lages, S., Unruh, T., Guldi, D.M., 2018. Excitons and trions in one-photon- and two-photon-excited MoS2: a study in dispersions. Adv. Mater 30, 1–10. https://doi.org/10.1002/adma.201706702.

Ai, K., Ruan, C., Shen, M., Lu, L., 2016. MoS2 nanosheets with widened interlayer spacing for high-efficiency removal of mercury in aquatic systems. Adv. Funct. Mater. 26, 5542–5549. https://doi.org/10.1002/adfm.201601338.

Jia, F., Zhang, X., Song, S., 2017a. AFM study on the adsorption of Hg2+ on natural molybdenum disulfide in aqueous solutions. Phys. Chem. Chem. Phys. 19, 3837–3844. https://doi.org/10.1039/C6CP07302F.

Jia, F., Liu, C., Yang, B., Zhang, X., Yi, H., Ni, J., Song, S., 2018. Thermal modification of molybdenum disulfide surface for tremendous improvement of Hg2+ adsorption from aqueous solution. ACS Sustain. Chem. Eng. 6, 9065–9073. https://doi.org/10.1021/acssuschemeng.8b01412.

Liu, C., Jia, F., Wang, Q., Yang, B., Song, S., 2017a. Two-dimensional molybdenum disulfide as adsorbent for high-efficient Pb(II) removal from water. Appl. Mater. Today 9, 220–228. https://doi.org/10.1016/j.apmt.2017.07.009.

Zhao, H., Yang, G., Gao, X., Pang, C.H., Kingman, S.W., Wu, T., 2015. Hg0 capture over CoMoS/ γ-Al2O3 with MoS2 nanosheets at low temperatures. Environ. Sci. Technol. 50, 1056–1065. https://doi.org/10.1021/acs.est.5b04278.

Peng, K., Fu, L., Li, X., Ouyang, J., Yang, H., 2017. Stearic acid modified montmorillonite as emerging microcapsules for thermal energy storage. Appl. Clay Sci. 138, 100–106. https://doi.org/10.1016/j.clay.2017.01.003.

Yuan, Y., Yang, B., Jia, F., Song, S., 2019. Reduction mechanism of Au metal ions into Au nanoparticles on molybdenum disulfide. Nanoscale 11, 9488–9497. https://doi.org/10.1039/c8nr09420a.

Wang, Z., Mi, B., 2017. Environmental applications of 2D molybdenum disulfide (MoS2) nanosheets. Environ. Sci. Technol. 51, 1–42. https://doi.org/10.1021/acs.est.7b01466.

Pető, J., Ollár, T., Vancsó, P., Popov, Z.I., Magda, G.Z., Dobrik, G., Hwang, C., Sorokin, P.B., Tapasztó, L., 2018. Spontaneous doping of the basal plane of MoS2 single layers through oxygen substitution under ambient conditions. Nat. Chem. 10, 1246–1251. https://doi.org/10.1038/s41557-018-0136-2.

Li, X., Peng, K., 2018. MoSe2/Montmorillonite composite nanosheets: hydrothermal synthesis, structural characteristics, and enhanced photocatalytic activity. Minerals 8, 268.

Liu, N., Kim, P., Kim, J.H., Ye, J.H., Kim, S.K., Lee, C.J., 2014. Large-area atomically thin MoS2 nanosheets prepared using electrochemical exfoliation. ACS Nano 8, 6902–6910.

Liu, C., Jia, F., Wang, Q., Yang, B., Song, S., 2017b. Two-dimensional molybdenum disulfide as adsorbent for high-efficient Pb(II) removal from water. Materialstoday 220–228.

Feng, Q., Wen, S., Deng, J., Zhao, W., 2017. Combined DFT and XPS investigation of enhanced adsorption of sulfide species onto cerussite by surface modification with chloride. Appl. Surf. Sci. 425, 8–15. https://doi.org/10.1016/j.apsusc.2017.07.017.

Feng, Q., Wen, S., Bai, X., Chang, W., Cui, C., Zhao, W., 2019. Surface modification of smithsonite with ammonia to enhance the formation of sulfidization products and its response to flotation. Miner. Eng. 137, 1–9. https://doi.org/10.1016/j.mineng.2019.03.021.

Feng, Q., Zhao, W., Wen, S., 2018. Surface modification of malachite with ethanediamine and its effect on sulfidization flotation. Appl. Surf. Sci. 436, 823–831. https://doi.org/10.1016/j.apsusc.2017.12.113.

Xie, J., Zhang, J., Li, S., Grote, F., Zhang, X., Zhang, H., Wang, R., Lei, Y., Pan, B., Xie, Y., 2013a. Controllable disorder engineering in oxygen-incorporated MoS2 ultrathin nanosheets for efficient hydrogen evolution. J. Am. Chem. Soc. 135, 17881–17888. https://doi.org/10.1021/ja408329q.

Xie, J., Sun, X., Zhang, N., Xu, K., Zhou, M., Xie, Y., 2013b. Layer-by-layer b -Ni (OH) 2 / graphene nanohybrids for ultraflexible all-solid-state thin-film supercapacitors with high electrochemical performance. Nano Energy 2, 65–74. https://doi.org/10.1016/j.nanoen.2012.07.016.

Zhang, X., Jia, F., Yang, B., Song, S., 2017. Oxidation of molybdenum disulfide sheet in water under in situ atomic force microscopy observation. J. Phys. Chem. C 121, 9938–9943. https://doi.org/10.1021/acs.jpcc.7b01863.

Sun, T., Li, Z., Liu, X., Ma, L., Wang, J., 2017. Oxygen-incorporated MoS2 microspheres

with tunable interiors as novel electrode materials for supercapacitors. J. Power Sources 352, 135–142. https://doi.org/10.1016/j.jpowsour.2017.03.123.
Liu, A., Zhao, L., Zhang, J., Lin, L., Wu, H., 2016. Solvent-assisted oxygen incorporation of vertically aligned MoS2 ultrathin nanosheets decorated on reduced graphene oxide for improved electrocatalytic hydrogen evolution. ACS Appl. Mater. Interfaces 8, 25210–25218. https://doi.org/10.1021/acsami.6b06031.
Huang, H., Feng, X., Du, C., Wu, S., Song, W., 2015. Incorporated oxygen in MoS2 ultrathin nanosheets for efficient ORR catalysis. J. Mater. Chem. A Mater. Energy Sustain. 3, 16050–16056. https://doi.org/10.1039/C5TA01600B.
Moo, S.H., Nanoarchitectures, G., Application, T., Material, H.A., Batteries, L., 2011. Self-assembled hierarchical MoO2 / graphene nanoarchitectures and their application as a high-performance anode material for lithium-ion. ACS Nano 5, 7100–7107.
Jia, F., Wang, Q., Wu, J., Li, Y., Song, S., 2017b. Two-dimensional molybdenum disulfide as a superb adsorbent for removing Hg2+ from water. ACS Sustain. Chem. Eng. 5, 7410–7419. https://doi.org/10.1021/acssuschemeng.7b01880.
Hyland, M.M., Jean, G.E., Bancroft, G.M., 1990. XPS and AES studies of Hg(II) sorption and desorption reactions on sulphide minerals. Geochim. Cosmochim. Acta 54, 1957–1967.
Yeong, H.Y., Sun, K., Hayes, K.F., 2010. Microscopic and spectroscopic characterization of Hg(II) immobilization by mackinawite(FeS). Environ. Sci. Technol. 44, 7476–7483.
Zeng, J., Yang, J., Qian, Y., 2001. A novel morphology controllable preparation method to HgS. Mater. R. 36, 343–348.
Zhao, C., Chen, J., Wu, B., Long, X., 2014. Density functional theory study on natural hydrophobicity of sulfide surfaces. Trans. Nonferrous Met. Soc. China 24, 491–498. https://doi.org/10.1016/S1003-6326(14)63087-9.
Peng, C., Min, F., Liu, L., Chen, J., 2016. DFT study of adsorption of water on sodium-montmorillonite (001) basal and (010) edge surface. Appl. Surf. Sci. 387, 308–316. https://doi.org/10.1016/j.apsusc.2016.06.079.